



Published in final edited form as:

*Meccanica*. 2017 February ; 52(3): 563–576. doi:10.1007/s11012-015-0322-x.

## Clinical assessment of intraventricular blood transport in patients undergoing cardiac resynchronization therapy

**Lorenzo Rossini,**

Mechanical and Aerospace Engineering Department, University of California San Diego, Mail Code 0411 9500 Gilman Drive, La Jolla, CA 92093, USA

**Pablo Martinez-Legazpi,**

Mechanical and Aerospace Engineering Department, University of California San Diego, Mail Code 0411 9500 Gilman Drive, La Jolla, CA 92093, USA; Department of Cardiology, Instituto de Investigación Sanitaria Gregorio Marañón, Hospital General Universitario Gregorio Marañón, Dr. Esquerdo 46, 28007 Madrid, Spain

**Yolanda Benito,**

Department of Cardiology, Instituto de Investigación Sanitaria Gregorio Marañón, Hospital General Universitario Gregorio Marañón, Dr. Esquerdo 46, 28007 Madrid, Spain

**Candelas Pérez del Villar,**

Department of Cardiology, Instituto de Investigación Sanitaria Gregorio Marañón, Hospital General Universitario Gregorio Marañón, Dr. Esquerdo 46, 28007 Madrid, Spain

**Ana Gonzalez-Mansilla,**

Department of Cardiology, Instituto de Investigación Sanitaria Gregorio Marañón, Hospital General Universitario Gregorio Marañón, Dr. Esquerdo 46, 28007 Madrid, Spain

**Alicia Barrio,**

Department of Cardiology, Instituto de Investigación Sanitaria Gregorio Marañón, Hospital General Universitario Gregorio Marañón, Dr. Esquerdo 46, 28007 Madrid, Spain

**María-Guadalupe Borja,**

Mechanical and Aerospace Engineering Department, University of California San Diego, Mail Code 0411 9500 Gilman Drive, La Jolla, CA 92093, USA

**Raquel Yotti,**

Department of Cardiology, Instituto de Investigación Sanitaria Gregorio Marañón, Hospital General Universitario Gregorio Marañón, Dr. Esquerdo 46, 28007 Madrid, Spain

**Andrew M. Kahn,**

Department of Medicine, University of California San Diego, La Jolla, CA, USA

**Shawn C. Shadden,**

Mechanical Engineering Department, University of California Berkeley, Berkeley, CA, USA

---

jalamo@ucsd.edu. javier.bermejo@salud.madrid.org.

Compliance with ethical standards

Conflict of interest None.

**Francisco Fernández-Avilés,**

Department of Cardiology, Instituto de Investigación Sanitaria Gregorio Marañón n, Hospital General Universitario Gregorio Marañón , Dr. Esquerdo 46, 28007 Madrid, Spain; Facultad de Medicina, Universidad Complutense de Madrid, Madrid, Spain

**Javier Bermejo, and**

Department of Cardiology, Instituto de Investigación Sanitaria Gregorio Marañón n, Hospital General Universitario Gregorio Marañón , Dr. Esquerdo 46, 28007 Madrid, Spain; Facultad de Medicina, Universidad Complutense de Madrid, Madrid, Spain

**Juan C. del Álamo**

Mechanical and Aerospace Engineering Department, University of California San Diego, Mail Code 0411 9500 Gilman Drive, La Jolla, CA 92093, USA, Institute for Engineering in Medicine, University of California San Diego, La Jolla, CA, USA

**Abstract**

In the healthy heart, left ventricular (LV) filling generates different flow patterns which have been proposed to optimize blood transport by coupling diastole and systole. This work presents a novel image-based method to assess how different flow patterns influence LV blood transport in patients undergoing cardiac resynchronization therapy (CRT). Our approach is based on solving the advection equation for a passive scalar field from time-resolved blood velocity fields. Imposing time-varying inflow boundary conditions for the scalar field provides a straightforward method to distinctly track the transport of blood entering the LV in the different filling waves of a given cardiac cycle, as well as the transport barriers which couple filling and ejection. We applied this method to analyze flow transport in a group of patients with implanted CRT devices and a group of healthy volunteers. Velocity fields were obtained using echocardiographic color Doppler velocimetry, which provides two-dimensional time-resolved flow maps in the apical long axis three-chamber view of the LV. In the patients under CRT, the device programming was varied to analyze flow transport under different values of the atrioventricular conduction delay, and to model tachycardia (100 bpm). Using this method, we show how CRT influences the transit of blood inside the left ventricle, contributes to conserving kinetic energy, and favors the generation of hemodynamic forces that accelerate blood in the direction of the LV outflow tract. These novel aspects of ventricular function are clinically accessible by quantitative analysis of color-Doppler echocardiograms.

**Keywords**

Blood transport; Intracardiac flow; Intraventricular flow patterns; Blood filling waves; Cardiac resynchronization therapy; Echocardiography

**1 Introduction**

Heart failure (HF) is an increasing global problem for healthcare systems. Responsible for high morbidity and mortality rates in developed countries, HF is the endpoint of a number of chronic cardiovascular diseases [1]. In more than half of patients with HF, the major hallmark of the disease is an impairment of systolic mechanics of the left ventricle (LV). The

disease evolution entails a progression of myocardial damage which may also affect the conduction system of the heart. If the conduction in the left-bundle-branch is functionally disturbed, the physiological pathway of normal LV activation is lost. By delaying the onset of mechanical systole of the LV free wall, left-bundle-branch block leads to a dyssynchronous contraction of the ventricular walls [2].

Dyssynchrony is associated with a higher risk of both worsened failure and sudden cardiac death [3]. In addition to intraventricular conduction abnormalities, patients with dyssynchrony also frequently have associated impaired conduction from the atria to the ventricles. Atrioventricular (AV) dyssynchrony further impairs the ability of the failing heart to pump blood, worsening the severity of HF [4–8].

Cardiac resynchronization therapy (CRT) is a well-established non-pharmacological treatment for congestive HF. CRT recovers the physiological activation pathways, improving cardiac function and clinical outcomes in patients who associate HF and dyssynchrony. When applied to adequately selected patient populations, CRT has a positive impact on symptoms, quality of life and mortality [9, 10]. This therapy is used to restore coordinated pumping of the ventricles by using a specialized cardiac pacemaker. Unfortunately, between 25 and 30 % of patients receiving CRT do not show the expected benefits. It has been suggested that achieving a favorable CRT response may in part depend on proper device programming [11–13]. Therefore, optimization of the AV delay has been shown to improve cardiac output and may be necessary in up to 55 % of CRT patients during follow-up [14–16]. However, the best method to optimize the AV delay is still controversial [17, 18].

Nature has optimized the coupling of molecular, electrical and mechanical processes of the heart, leading to flow patterns that minimize energy losses and facilitate the smooth redirection of incoming blood towards the outflow tract [19–22]. The interaction between wall mechanics and intracavitary flow establishes fluid transport barriers, which separate the blood that transits from inflow directly to outflow each cardiac cycle from the blood that is retained inside the LV [22–26]. Lagrangian particle tracking using time-resolved 3D phase-contrast MRI velocity fields [27] and analysis of Lagrangian coherent structures (LCS) have been instrumental to quantify these transport barriers [22, 28]. However, these methods are based on expensive calculations of the trajectories of virtual fluid particles, and are difficult to automate for high-throughput analysis in the clinical setting.

Preliminary studies have shown that the main intraventricular flow pattern, a vortex ring that forms during diastole, is highly sensitive to the timing intervals of the cardiac cycle and to tachycardia [29]. Shortening the filling period by programming long electrical AV delays increases the circulation and kinetic energy of the vortex and results in the vortex staying closer to the mitral valve [28]. When compared to baseline conduction, biventricular stimulation seems to improve organization of intraventricular flow, suggesting that intraventricular flow analysis is a useful tool to understand the effects of resynchronization on heart mechanics [30]. Remarkably, changes in electrical activation have been shown to modify the net orientation of the forces acting on blood inside the LV, which has been associated with improved long-term outcome in patients undergoing CRT [31]. These findings suggest that flow imaging may be a suitable tool for optimizing this therapy.

However, how CRT settings affect the specific time evolution of the different flow volumes and the LV filling waves is still poorly understood.

The present study was designed with the twofold purpose of (1) implementing a clinically feasible high-throughput method for measuring and mapping blood transport in the heart, and (2) testing its clinical potential to characterize changes in blood transport caused by CRT. The general approach was to obtain individual quantitative metrics of flow transport from flow-velocity measurements in the LV.

## 2 Methods

### 2.1 Study population

The present study is based on the analysis of 9 patients with HF and CRT under different AV delays and 3 healthy volunteers matched by age and gender to the patient group. Patients were consecutively enrolled from the pacemaker outpatient clinic. Controls were selected from a large database of healthy volunteers recruited at our institutions [32]. The study protocol was approved by the local institutional review committee, and all subjects provided written informed consent for this study. Clinical data are summarized in Table 1.

### 2.2 Reproducibility analysis

Reproducibility analysis of the processed data was performed in seven subjects randomly selected from a large Doppler Echocardiographic study database. Inclusion was based on the absence of known or suspected cardiovascular disease, a normal EKG, a normal Doppler-echocardiographic exam, and no history of hypertension or diabetes.

### 2.3 AV delay settings and data acquisition

In the patient group, ultrasound sequences were acquired at 5 different programming settings to analyze the effect of pacing (CRT on vs CRT off), the AV delay and the heart rate. Patients were studied in spontaneous sinus rhythm at 3 different AV delay settings: maximum AV (AVMAX), minimum AV (AVMIN), optimum AV (AVOPT). Then, maintaining the optimum AV delay, images were again acquired at 100 bpm induced by atrial pacing. Finally, patients were studied after turning off the cardiac pacing (CRTOFF). Maximum AV delay was obtained by increasing AV delay until capture was lost due to intrinsic conduction. Minimum AV delay was obtained by decreasing it down to 80 ms. The optimum AV delay was set using the iterative method, which uses the mitral valve pulsed wave Doppler to optimize the diastolic filling time (DFT). The iterative method attempts to obtain the longest DFT time that does not truncate the A-wave, achieving maximal separation between the E- and the A-waves. Briefly, DFT was measured from the start of the E-wave until the end of the A-wave. A long AV delay was programmed and reduced in 20-ms steps until A-wave truncation. The interval was then increased in 10 ms increments, and the shortest AV delay without A-wave truncation was selected to maximize the DFT [12].

Comprehensive echocardiographic examinations were performed using a Vivid 7 ultrasound machine with 2–4 MHz transducers (GE Healthcare). For each particular CRT-device setting, we obtained 2D color-Doppler and B-mode (grayscale) sequences from the long-axis

apical view. In addition, pulsed-wave Doppler recordings were obtained from the 5-chamber apical view, carefully located to obtain spectral recordings of opening and closing of the mitral and aortic valves. Event timings of the cardiac cycle were measured from these recordings, and then forwarded to the fluid-dynamic solver [32].

### 3 2D Image analysis and intraventricular flow processing

The LV myocardial wall was segmented using speckle-tracking software to delineate the endocardial boundary (EchoPac v.110.1.2, GE Healthcare). We reconstructed the time-dependent flow field inside the LV using 2D echo-CDV, as previously described and validated in vitro [33] and in vivo [32]. Conventional Doppler-echocardiographic data was measured following current recommendations [34].

#### 3.1 Blood transport assessment

**3.1.1 Blood transport equation for virtual multi-color angiography**—Using the time-dependent 2D echo-CDV velocity field  $\mathbf{v}(\mathbf{x},t)$  and the LV wall tracking data as input, we solved an advection equation for a passive scalar field  $\psi$  with uniform initial conditions and step-wise Dirichlet inflow boundary conditions,

$$\begin{aligned} \frac{D\psi}{Dt} &= \partial_t \psi + \nabla \cdot (\mathbf{v}\psi) = 0, \\ \psi(\mathbf{x}, t = 0) &= \psi_0 = \text{const}, \\ \psi(\mathbf{x}_{inlet}, 0 < t < t_1) &= \psi_1 = \text{const}, \\ \psi(\mathbf{x}_{inlet}, t_1 \leq t < t_2) &= \psi_2 = \text{const}, \\ &\text{etc.} \end{aligned} \quad (1)$$

This continuous semi-Lagrangian approach tags different volumes of blood with different numerical values that are transported by the flow, thereby simulating the visualization of distinct virtual contrast media inside the LV. For instance, one can implement a two-step inlet boundary condition to track the evolution of the two fluid volumes that enter the ventricle during the E wave and the A wave. Blood is a complex multi-component suspension for which it is generally accepted that the mass diffusivity of different species is negligible compared to momentum diffusivity [35, 36]. Thus, we did not include a diffusive term in the transport equation. This approach is analogous to previous analyses of LV blood transport based on the deterministic integration of fluid particle trajectories [22–26, 28]. Note that the absence of diffusive terms makes it possible to integrate Eq. 1 backward in time, applying Dirichlet boundary conditions at the outlet of the domain. As shown below, combining the results from the forward and backward integrations allows for a straightforward categorization of blood transport templates inside the LV. Equation (1) was numerically integrated using previously described in-house software written in FORTRAN [37]. The equation was discretized on a Cartesian grid by a 2nd-order finite volume method, and a total variation diminishing flux limiting scheme was used to avoid numerical oscillations at the sharp interfaces created between volumes of blood with different inflow tags.

**3.1.2 Characterization of blood transport patterns**—The time-evolving distribution of  $\psi$  was automatically thresholded to separate and track the blood carried by the transport structures generated during the E-wave and A-wave, and to determine the size of these structures and their frontal position. Equation (1) was integrated with uniform initial conditions and two different inlet boundary conditions for the E wave and A wave (e.g.  $\psi(\mathbf{x}, t=0) = 0$ ,  $\psi(\mathbf{x}_{inlet}, t \in Ewave) = 1$  and  $\psi(\mathbf{x}_{inlet}, t \in Awave) = 2$ ). The iso-contours  $\psi = 0, 1, 2$  allowed us to track the time-evolving distribution of the blood that entered the LV during both filling waves, together with that of the residual volume of blood occupying the LV at the onset of diastole. E and A wave sizes,  $S_E$  and  $S_A$ , were calculated from the area they occupied in the imaging plane, and normalized by the total end-diastolic LV area in the same plane. To systematically analyze the effect of AV delay on LV filling transport, we determined the fraction of LV size occupied by the E and A waves,  $S_E/S_{LV}$  and  $S_A/S_{LV}$ , as well as the normalized apical position of each wave's front  $X_E/L$  and  $X_A/L$ , where  $L$  is the long axis length of the LV (i.e.  $X/L = 0$  is the LV base and  $X/L = 1$  is the LV apex).

In addition to tracking the filling transport patterns, we analyzed the spatiotemporal evolution of the blood that is ejected each cardiac cycle by integrating Eq. (1) backwards in time with uniform initial conditions, and Dirichlet boundary conditions at the aortic valve annulus. Combining the results from the backward and forward integrations allowed us to automatically identify the following transport structures: direct flow (DF, blood that enters and exits the LV in the same cardiac cycle), retained inflow (RI, incoming blood that is not ejected during the same cycle), delayed ejection (DE, ejected blood that entered the LV in a previous cardiac cycle) and residual flow (RF, blood that entered the LV in a previous cycle and is not ejected in the current cycle, therefore residing in the LV for at least two cardiac cycles) [22]. For the purpose of this 2D study we used the respective planar-volumes (areas) to account for each of these fractions.

To assess the kinematic efficiency of flow redirection inside the LV under CRT, we determined the size, kinetic energy density and acceleration of each transport region at the onset of systole. Kinetic energy density was calculated from 2D echo-CDV data as  $K(\mathbf{x}, t) = |\mathbf{v}|^2/2$ . Fluid acceleration was calculated as  $\mathbf{m}(\mathbf{x}, t_0) = \left(\frac{\partial \mathbf{v}}{\partial t} + \mathbf{v} \cdot \nabla \mathbf{v}\right)$ . These variables were spatially integrated over the surface occupied by each transport region to obtain their overall values inside the region (e.g.  $\mathbf{M}_{DF} = \int_{S_{DF}} \mathbf{m}(\mathbf{x}) d\mathbf{x}$ ). It is important to note that  $\mathbf{M}$  is a vector that not only indicates the magnitude of the acceleration of each fluid volume, but also its direction. The orientation of the whole ventricle's  $\mathbf{M}$  with respect with the ventricular long axis has been recently shown to correlate with long-term outcome in patients undergoing CRT [31]. We calculated the ratio  $\eta_K = K_{DF}/K_{LV}$  at aortic valve opening in all the patients to determine if CRT changes contributed to efficiently focusing the inflow kinetic energy into the volume of fluid that was ejected during systole. The ratio of direct flow area to total LV area in the imaging plane,  $\eta_{DF} = S_{DF}/S_{LV}$ , was also computed to quantify the efficiency of volumetric blood transport within one cardiac cycle.

In addition to focusing kinetic energy into the direct flow volume, efficient LV blood transit from the inflow to the outflow tract requires a marked change in the direction of fluid motion. A measure of the efficiency of this process is the net acceleration transferred to the



direct flow region in the direction of the LV outflow tract normalized with the total magnitude of this acceleration,  $\eta_M = (M_{DF} \cdot e_{LVOT})/|M_{DF}|$ , where  $e_{LVOT}$  is the unitary vector parallel to the direction of the LV outflow tract, pointing outwards the LV. The calculation of the 2D + t velocity field, the integration of Eq. (1) and the post processing work were programmed to be automatic and operator-independent. Best and worst full time for the entire post-processing from RAW echo images were 10 and 20 min ( $13 \pm 3$  min).

Reproducibility (fully blinded echocardiographic image acquisition and re-acquisition, calculation of 2D flow velocity fields, event-time identification, and final index computation by two independent observers;  $n = 7$  normal subjects) was relatively good for most calculated indices (Table 2).

### 3.2 Statistical analysis

Individual scatterplots and boxplots showing the median and interquartile range are shown for each parameter. Differences among phases are compared using linear mixed effects accounting for repeated measured within each subject (random effect). Reproducibility of quantitative indices was analyzed using the intraclass correlation coefficient ( $R_{iC}$ ). All analyses were performed in R (v. 3.2) and  $p$  values  $<0.05$  were considered significant.

## 4 Results

### 4.1 Intraventricular inflow and blood transport under cardiac resynchronization therapy

CRT and AV delay optimization modify the inflow velocity profile in patients implanted with bi-ventricular pacemakers. This is illustrated in Fig. 1, which displays pulsed wave Doppler (PW) measurements from a representative patient (CRT7, see Table 1) for each one of the 5 different pacing settings. The PW profiles exhibit the two flow velocity envelopes that define left-ventricular filling flow: the E-wave representing the early, passive filling phase of the LV, and the A-wave representing the late active filling phase driven by atrial contraction. Varying the AV delay displaces the start and end of these waves in time, and modulates the magnitude and timing of the inflow velocity, leading therefore to different intraventricular flow fields.

### 4.2 Atrioventricular delay and blood transport during early and late filling

The AV delay has a number of effects not only on global chamber mechanics but also on myocardial fiber pre-stretching and contraction [38]. Consequently, as said above, changes in AV delay modify the dynamics of the filling flow driven by the E and A waves. Figure 2 illustrates these differences for the same patient shown in Fig. 1. The total amount of blood entering the LV varied between 26 and 42 % of the LV area in the imaged plane for the pacing settings considered, in fair agreement with the patient's measured ejection fraction of 29 % measured at AVOPT. More importantly, both the size (i.e. area) and shape of the regions defined by E-wave and A-wave filling were sensitive to the presence of pacing (CRTON vs CRTOFF), the AV delay, and the heart rate (Table 3). In the patient group, CRT increased the fraction of LV volume occupied by the E wave at the end of diastole, bringing this variable closer to the healthy range (Fig. 3a). The observed increase in early LV filling volume was particularly noticeable for AVOPT, where 6 out of the 9 patients experienced an

increase in  $S_E/S_{LV}$ . We found a similar trend for CRT to increase the apical position of the E-wave front (Table 3). Moreover, CRT caused a moderate increase in the late filling volume fraction  $S_A/S_{LV}$  (Fig. 3b).

### 4.3 Time-evolution of intraventricular transport regions

Figure 4 displays the end-diastolic distribution of the direct flow, retained inflow, delayed ejection and residual flow regions in the LV of the representative patient shown in Figs. 1 and 2. In the absence of pacing, the overall transit of LV blood transport followed a wide arch, so that a large fraction of LV volume in the center of the chamber remained as residual flow. CRT altered this effect increasing direct flow, particularly for AVOPT. With tachycardia, the filling and ejection phases were shortened and defined small transport regions that did not intersect significantly, consequently creating a small amount of direct flow. Figure 5a and Table 4 summarize the statistics of  $\eta_{DF}$  (ratio of direct flow area to total LV area) as a function of AV delay in the patient population, including reference data from healthy subjects and previous studies. Consistent with Fig. 4, AVOPT shows a significant increment in the direct flow region with respect to the CRTOFF condition in the whole population;  $\eta_{DF}$  increased in 7 of the 9 patients, and the median  $\eta_{DF}$  increased by a factor of  $\sim 3$ . The variation of  $\eta_{DF}$  was less pronounced for the two other AV delay settings, though  $\eta_{DF}$  increased in 7 out of 9 patients for both AVMIN and AVMAX. In addition to increasing direct flow, CRT enhanced the efficiency of LV blood transit by decreasing the portion of the chamber occupied by residual volume, defined as  $\lambda_{RF} = S_{RF}/S_{LV}$  (Fig. 5b). Eight out of 9 patients reduced their residual volumes at AVOPT. Nevertheless, AVMAX also provided a significant effect ( $\lambda_{RF}$  decreased in 7/9 patients). Reproducibility test–retest for all the volumetric indices ( $\eta_{DF}$ ,  $S_{RI}/S_{LV}$ ,  $S_{DE}/S_{LV}$ ,  $\lambda_{RF}$ ,  $S_E/S_{LV}$ , and  $S_A/S_{LV}$ ) showed fair agreement both in the intraobserver and interobserver analysis (Table 2).

We found  $\eta_K$  (ratio of direct flow kinetic energy to total LV total kinetic) to be higher in the healthy subjects than in the patients with CRTOFF. Furthermore, there was a clear trend of increase in  $\eta_K$  with CRT that was relatively insensitive to the AV delay. Additionally, CRT decreased the amount of inflow kinetic energy that remained in the residual volume at the end of diastole,  $\lambda_K = K_{RF}/K_{LV}$ . The observed decrease in wasted kinetic energy was most significant for AVOPT and AVMIN, with  $\lambda_K$  showing variations in 8 and 9 (out of 9) patients respectively (Fig. 5d; Table 5).

Figure 5e and Table 5 summarize the statistics of  $\eta_M$  (fraction of direct flow acceleration in the direction of the LV outflow tract) at the onset of systole. Similar to  $\eta_{DF}$  and  $\eta_K$ , this directional parameter efficiency became higher with CRT regardless of the AV delay, showing an increase in 6 out of 9 patients for AVMIN, AVMAX and AVOPT.

## 5 Discussion

In the present study we implement a high-throughput method, suitable for visualizing and measuring flow transport in the LV using ultrasound in the clinical setting. This method is based on a continuous semi-Lagrangian formulation that allowed us to track and to determine quantitative metrics of LV volume fractions from flow velocity measurements with no user interaction. As a result, this method provides accurate maps of blood transport



without the need to integrate the trajectories of a large number of virtual blood particles and to perform semi-manual segmentation of the delineated fluid structures, as previously done using either phase-contrast MR [22] or Doppler-echocardiography [28]. Our data compare well with previous studies using phase-contrast MR in healthy and diseased hearts, as shown in Table 4.

We used manual modification of CRT pacemaker parameters to illustrate the clinical potential of this novel tool, and demonstrated acute changes in blood transport patterns inside the LV with different AV delays. As shown, flow organization inside the LV is highly dynamic and sensitive to the timing of cardiac events. Even a moderate increase in heart rate induced important changes in the manner LV flow affects the transit of blood from the mitral valve to the aorta.

However, the functional consequences of intraventricular flow organization remain mostly unknown. It has been shown that diastolic vortex structures are useful to efficiently transport flow from the LA towards the apex, both during the early and late filling phases [39, 40]. As described above, direct flow allows a significant amount of the inflow's kinetic energy to be transferred to the ejection volume. To what extent preserving energy throughout the cardiac cycle provides a functional benefit in the normal heart is a matter of debate [10, 19, 41, 42]. However, any mechanism of increased performance may be relevant in the failing ventricle which has almost exhausted its contractile reserve.

Overall, the presented data imply that the spatiotemporal evolution of the intraventricular blood flow in patients undergoing CRT can be highly sensitive to heart rate and AV delay. The blood flow in the CRT OFF condition is driven by a persistent clockwise swirling pattern that is typically found in patients with dilated cardiomyopathy [28, 32], forcing the blood entering the LV to follow an arched path along the inferolateral and anteroseptal LV walls. Turning CRT on modified this transport pattern, particularly for AVOPT. For the latter CRT setting, the incoming blood was distributed forming a pattern consistent with a more symmetric starting jet—vortex ring structure.

In addition to having an effect on LV filling, CRT may potentially improve the efficient redirection of left ventricular blood inflow towards the outflow tract by: (1) modifying the transport patterns to increase the amount of blood coming into the LV each cardiac cycle that is ejected in the same cardiac cycle (i.e. direct flow), (2) increasing the amount of kinetic energy that is transferred from incoming blood to ejected blood, and (3) aligning the motion of the ejected blood with the left ventricular outflow tract. Furthermore, our results and the emerging literature imply that CRT favors the generation of coherent intraventricular pressure gradients that accelerate blood in the direction of the LV outflow tract [31]. Finally, the impact of different transport patterns on intraventricular flow mixing and prevention of blood stasis needs to be addressed [37].

Flow transport visualization methods such as the one presented in this study are readily applicable to large patient populations and are therefore particularly well suited to clarify issues such as the effect of CRT on LV blood transport. This is supported by the relatively good agreement between the presented data and previous studies using PC-MR, especially in

the diseased heart (see Table 4). From a clinical perspective, this method opens the possibility of using flow imaging techniques to optimize CRT. However, large-scale trials will be necessary to clarify the future role of intracardiac fluid dynamics in medical diagnosis, clinical decision-making, and physiologic programming of cardiac devices. In addition, these emerging methods will likely provide new fundamental insight on cardiac biomechanics. Flow transport visualization methods not only will help investigators to understand the physiological basis of heart failure but also to optimize pharmacological and non-pharmacological therapies to improve the outcomes associated with one of the most prevalent diseases in the world.

## 6 Limitations

We used a 2D flow imaging method even though intraventricular blood transport is a 3D process. This planar flow simplification may lead to some degree of inaccuracy in the estimation of transport. However, our echocardiographic 2D approach has important practical advantages, as it provides high temporal and spatial resolutions, is fast, clinically feasible, and does not require infusion of contrast agents. Moreover, the proposed transport analysis methodology relies on clinical access to time-resolved LV velocity fields, but it is independent of the particular imaging modality employed to measure intraventricular velocity. Applying a similar analysis to flow velocity maps from time-resolved 3D phase-contrast MR has shown that the key features of intraventricular blood transport and mixing are well represented in the long-axis three-chamber plane imaged by 2D echo-CDV [43]. Thus, although the exact transport numerical values may vary when they are calculated in 3D, we are confident that our 2D analysis was able to accurately capture relative changes induced by CRT on intraventricular flow transport. Larger clinical studies shall establish the final clinical role of this novel methodology technique in the modern armamentarium of cardiovascular imaging.

## 7 Conclusions

Blood transport patterns in the LV can be readily derived from flow-velocity fields by solving a passive-scalar advection partial differential equation. This continuous semi-Lagrangian method is suitable for high-throughput processing without the need of discrete particle tracking or user interaction. Combining this tool with color-Doppler ultrasound, we were able to demonstrate important effects of cardiac resynchronization therapy and atrioventricular delay optimization on intraventricular blood transport.

## Acknowledgments

This study was supported by grants, PI12/02885, PIS09/02603, RD12/0042 (Red de Investigación Cardiovascular), and CM12/00273 (to CPV) from the Instituto de Salud Carlos III –Ministerio de Economía y Competitividad, Spain, and NIH grant 1R21 HL108268–01 (to JCA and AMK).

## References

1. Guha K, McDonagh T (2013) Heart failure epidemiology: European perspective. *Curr Cardiol Rev* 9(2):123–127 [PubMed: 23597298]

2. Farwell D, Patel NR, Hall A, Ralph S, Sulke AN (2000) How many people with heart failure are appropriate for biventricular resynchronization? *Eur Heart J* 21(15):1246–1250. doi:10.1053/euhj.1999.1985 [PubMed: 10924314]
3. Kass DA (2005) Cardiac resynchronization therapy. *J Cardiovasc Electrophysiol* 16(Suppl 1):S35–S41. doi:10.1111/j.1540-8167.2005.50136.x [PubMed: 16138884]
4. Xiao HB, Roy C, Fujimoto S, Gibson DG (1996) Natural history of abnormal conduction and its relation to prognosis in patients with dilated cardiomyopathy. *Int J Cardiol* 53(2):163–170 [PubMed: 8682602]
5. Xiao HB, Brecker SJ, Gibson DG (1992) Effects of abnormal activation on the time course of the left ventricular pressure pulse in dilated cardiomyopathy. *Br Heart J* 68(4):403–407 [PubMed: 1449925]
6. Littmann L, Symanski JD (2000) Hemodynamic implications of left bundle branch block. *J Electrocardiol* 33(Suppl):115–121 [PubMed: 11265710]
7. Saxon LA, Kerwin WF, Cahalan MK, Kalman JM, Olgin JE, Foster E, Schiller NB, Shinbane JS, Lesh MD, Merrick SH (1998) Acute effects of intraoperative multisite ventricular pacing on left ventricular function and activation/contraction sequence in patients with depressed ventricular function. *J Cardiovasc Electrophysiol* 9(1):13–21 [PubMed: 9475573]
8. Kerwin WF, Botvinick EH, O'Connell JW, Merrick SH, DeMarco T, Chatterjee K, Scheibly K, Saxon LA (2000) Ventricular contraction abnormalities in dilated cardiomyopathy: effect of biventricular pacing to correct interventricular dyssynchrony. *J Am Coll Cardiol* 35(5):1221–1227 [PubMed: 10758964]
9. Bristow MR, Saxon LA, Boehmer J, Krueger S, Kass DA, De Marco T, Carson P, DiCarlo L, DeMets D, White BG, DeVries DW, Feldman AM, Investigators C (2004) Cardiac-resynchronization therapy with or without an implantable defibrillator in advanced chronic heart failure. *N Engl J Med* 350(21):2140–2150 [PubMed: 15152059]
10. Pedrizzetti G, Domenichini F (2005) Nature optimizes the swirling flow in the human left ventricle. *Phy Rev Lett* 95(10):108101
11. Gorcsan J 3rd, Abraham T, Agler DA, Bax JJ, Derumeaux G, Grimm RA, Martin R, Steinberg JS, Sutton MS, Yu CM, American Society of Echocardiography Dyssynchrony Writing G, American Society of Echocardiography Dyssynchrony Writing G, Heart Rhythm S (2008) Echocardiography for cardiac resynchronization therapy: recommendations for performance and reporting—a report from the American Society of Echocardiography Dyssynchrony Writing Group endorsed by the Heart Rhythm Society. *J Am Soc Echocardiogr* 21(3):191–213. doi:10.1016/j.echo.2008.01.003 [PubMed: 18314047]
12. Stanton T, Hawkins NM, Hogg KJ, Goodfield NE, Petrie MC, McMurray JJ (2008) How should we optimize cardiac resynchronization therapy? *Eur Heart J* 29(20):2458–2472. doi:10.1093/eurheartj/ehn380 [PubMed: 18755703]
13. Pavlopoulos H, Nihoyannopoulos P (2010) Recent advances in cardiac resynchronization therapy: echocardiographic modalities, patient selection, optimization, non-responders—all you need to know for more efficient CRT. *Int J Cardiovasc Imaging* 26(2):177–191. doi:10.1007/s10554-009-9523-5 [PubMed: 19937388]
14. Waggoner AD, De Las Fuentes L, Faddis MN, Gleva MJ, Spence KE, Davila-Roman VG (2008) Left ventricular diastolic filling prior to cardiac resynchronization therapy: implications for atrioventricular delay programming. *Pacing Clin Electrophysiol* 31(7):838–844. doi:10.1111/j.1540-8159.2008.01097.x [PubMed: 18684280]
15. Zhang Q, Fung JWH, Chan YS, Chan HCK, Lin H, Chan S, Yu CM (2008) The role of repeating optimization of atrioventricular interval during interim and long-term follow-up after cardiac resynchronization therapy. *Int J Cardiol* 124(2):211–217. doi:10.1016/j.ijcard.2007.02.043 [PubMed: 17442425]
16. Auricchio A, Stellbrink C, Sack S, Block M, Vogt J, Bakker P, Huth C, Schondube F, Wolfhard U, Bocker D, Krahnfeld O, Kirkels H, Pacing Therapies in Congestive H (2002) Long-term clinical effect of hemodynamically optimized cardiac resynchronization therapy in patients with heart failure and ventricular conduction delay. *J Am Coll Cardiol* 39(12):2026–2033 [PubMed: 12084604]

17. Sawhney NS, Waggoner AD, Garhwal S, Chawla MK, Osborn J, Faddis MN (2004) Randomized prospective trial of atrioventricular delay programming for cardiac resynchronization therapy. *Heart Rhythm* 1(5):562–567. doi:10.1016/j.hrthm.2004.07.006 [PubMed: 15851220]
18. Kedia N, Ng K, Apperson-Hansen C, Wang CH, Tchou P, Wilkoff BL, Grimm RA (2006) Usefulness of atrioventricular delay optimization using Doppler assessment of mitral inflow in patients undergoing cardiac resynchronization therapy. *Am J Cardiol* 98(6):780–785 [PubMed: 16950184]
19. Kilner PJ, Yang GZ, Wilkes AJ, Mohiaddin RH, Firmin DN, Yacoub MH (2000) Asymmetric redirection of flow through the heart. *Nature* 404(6779):759–761 [PubMed: 10783888]
20. Richter YEE (2006) Cardiology is flow. *Circulation* 113(23):2679–2682 [PubMed: 16769924]
21. Yang GZ, Merrifield R, Masood S, Kilner PJ (2007) Flow and myocardial interaction: an imaging perspective. *Philos Trans R Soc Lond B Biol Sci* 362(1484):1329–1341. doi:10.1098/rstb.2007.2119 [PubMed: 17584731]
22. Bolger AF, Heiberg E, Karlsson M, Wigstrom L, Engvall J, Sigfridsson A, Ebberts T, Kvitting JP, Carlhall CJ, Wranne B (2007) Transit of blood flow through the human left ventricle mapped by cardiovascular magnetic resonance. *J Cardiovasc Magn Reson* 9(5):741–747 [PubMed: 17891610]
23. Fredriksson AG, Zajac J, Eriksson J, Dyverfeldt P, Bolger AF, Ebberts T, Carlhall CJ (2011) 4-D blood flow in the human right ventricle. *Am J Physiol Heart Circ Physiol* 301(6):H2344–H2350. doi:10.1152/ajpheart.00622.2011 [PubMed: 21926347]
24. Eriksson J, Dyverfeldt P, Engvall J, Bolger AF, Ebberts T, Carlhall CJ (2011) Quantification of presystolic blood flow organization and energetics in the human left ventricle. *Am J Physiol Heart Circ Physiol* 300(6):H2135–H2141. doi:10.1152/ajpheart.00993.2010 [PubMed: 21421820]
25. Eriksson J, Carlhall CJ, Dyverfeldt P, Engvall J, Bolger AF, Ebberts T (2010) Semi-automatic quantification of 4D left ventricular blood flow. *J Cardiovasc Magn Reson* 12:9. doi: 10.1186/1532-429X-12-9 [PubMed: 20152026]
26. Eriksson J, Bolger AF, Ebberts T, Carlhall CJ (2013) Four-dimensional blood flow-specific markers of LV dysfunction in dilated cardiomyopathy. *Eur Heart J Cardiovasc Imaging* 14(5):417–424. doi: 10.1093/ehjci/jes159 [PubMed: 22879457]
27. Wigstrom L, Ebberts T, Fyrenius A, Karlsson M, Engvall J, Wranne B, Bolger AF (1999) Particle trace visualization of intracardiac flow using time-resolved 3D phase contrast MRI. *Magn Reson Med* 41(4):793–799 [PubMed: 10332856]
28. Hendabadi S, Bermejo J, Benito Y, Yotti R, Fernandez-Aviles F, Del Alamo JC, Shadden SC (2013) Topology of blood transport in the human left ventricle by novel processing of Doppler echocardiography. *Ann Biomed Eng* 41(12):2603–2616. doi:10.1007/s10439-013-0853-z [PubMed: 23817765]
29. Benito Y, Bermejo J, Alhama M, Yotti R, Pérez del Villar C, Martínez-Legazpi P, González-Mansilla A, Barrio A, Fernández-Avilés F, del Álamo JC (2012) Heart rate and AV delay modify left ventricular filling vortex properties. *Circulation* 126:A18099
30. Goliasch G, Goscinska-Bis K, Caracciolo G, Nakabo A, Smolka G, Pedrizzetti G, Narula J, Sengupta PP (2013) CRT improves LV filling dynamics: insights from echocardiographic particle imaging velocimetry. *JACC Cardiovasc Imaging* 6(6):704–713. doi:10.1016/j.jcmg.2013.04.004 [PubMed: 23764097]
31. Pedrizzetti G, Martiniello AR, Bianchi V, D’Onofrio A, Caso P, Tonti G (2015) Changes in electrical activation modify the orientation of left ventricular flow momentum: novel observations using echocardiographic particle image velocimetry. *Eur Heart J Cardiovasc Imaging* doi:10.1093/ehjci/jev137
32. Bermejo J, Benito Y, Alhama M, Yotti R, Martinez-Legazpi P, Pérez del Villar C, Pérez-David E, González-Mansilla A, Santa-Marta C, Barrio A, Fernandez-Aviles F, del Alamo JC (2014) Intraventricular vortex properties in non-ischemic dilated cardiomyopathy. *Am J Physiol Heart Circ Physiol* 306(5):H718–H729. doi:10.1152/ajpheart.00697.2013 [PubMed: 24414062]
33. Garcia D, Del Alamo JC, Tanne D, Yotti R, Cortina C, Bertrand E, Antoranz JC, Perez-David E, Rieu R, Fernandez-Aviles F, Bermejo J (2010) Two-dimensional intraventricular flow mapping by digital processing conventional color-Doppler echocardiography images. *IEEE Trans Med Imaging* 29(10):1701–1713. doi:10.1109/tmi.2010.2049656 [PubMed: 20562044]

34. Lang RM, Badano LP, Mor-Avi V, Afilalo J, Armstrong A, Ernande L, Flachskampf FA, Foster E, Goldstein SA, Kuznetsova T, Lancellotti P, Muraru D, Picard MH, Rietzschel ER, Rudski L, Spencer KT, Tsang W, Voigt JU (2015) Recommendations for cardiac chamber quantification by echocardiography in adults: an update from the American Society of Echocardiography and the European Association of Cardiovascular Imaging. *J Am Soc Echocardiogr* 28 (1):1–39 e14. doi: 10.1016/j.echo.2014.10.003 [PubMed: 25559473]
35. Bermejo J, Martinez-Legazpi P, del Alamo JC (2015) The Clinical Assessment of Intracardiac Flows. *Ann Rev Fluid Mech* 47:315–342. doi:10.1146/annurev-fluid-010814-014728
36. Tarbell JM (2003) Mass transport in arteries and the localization of atherosclerosis. *Annu Rev Biomed Eng* 5:79–118. doi:10.1146/annurev.bioeng.5.040202.121529 [PubMed: 12651738]
37. Rossini L, Martinez-Legazpi P, Vu V, Fernández-Friera L, Pérez del Villar C, Rodríguez-López S, Benito Y, Borja M-G, Pastor-Escuredo D, Yotti R, Ledesma-Carbayo MJ, Kahn AM, Ibáñez B, Fernández-Avilés F, May-Newman K, Bermejo J, del Alamo JC (2015) A clinical method for mapping and quantifying blood stasis in the left ventricle. *J Biomech* doi:10.1016/j.jbiomech.2015.11.049
38. Zwanenburg JJ, Gotte MJ, Kuijjer JP, Hofman MB, Knaapen P, Heethaar RM, van Rossum AC, Marcus JT (2005) Regional timing of myocardial shortening is related to prestretch from atrial contraction: assessment by high temporal resolution MRI tagging in humans. *Am J Physiol Heart Circ Physiol* 288(2):H787–H794 [PubMed: 15486034]
39. Gharib M, Rambod E, Kheradvar A, Sahn DJ, Dabiri JO (2006) Optimal vortex formation as an index of cardiac health. *Proc Natl Acad Sci USA* 103(16):6305–6308. doi:10.1073/pnas.0600520103 [PubMed: 16606852]
40. Martinez-Legazpi P, Bermejo J, Benito Y, Yotti R, Perez Del Villar C, Gonzalez-Mansilla A, Barrio A, Villacorta E, Sanchez PL, Fernandez-Aviles F, del Alamo JC (2014) Contribution of the diastolic vortex ring to left ventricular filling. *J Am Coll Cardiol* 64(16):1711–1721. doi:10.1016/j.jacc.2014.06.1205 [PubMed: 25323260]
41. Seo JH, Mittal R (2013) Effect of diastolic flow patterns on the function of the left ventricle. *Phys Fluids* 25:110801
42. Watanabe H, Sugiura S, Hisada T (2008) The looped heart does not save energy by maintaining the momentum of blood flowing in the ventricle. *Am J Physiol Heart Circ Physiol* 294(5):H2191–H2196. doi:10.1152/ajpheart.00041.2008 [PubMed: 18326797]
43. Thompson RB, McVeigh ER (2003) Fast measurement of intracardiac pressure differences with 2D breath-hold phase-contrast MRI. *Magn Reson Med* 49(6):1056–1066 [PubMed: 12768584]

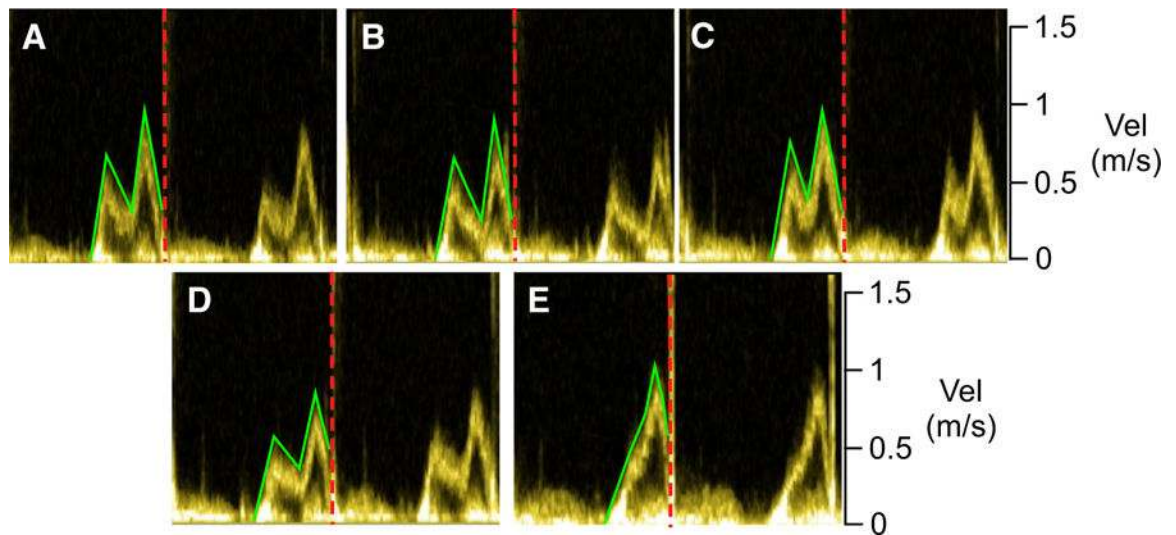


**Fig. 1.** Pulse wave Doppler inflow velocity as a function of time in a patient without CRT (a), and undergoing CRT at AVOPT (b), AVMAX (c), AVMIN (d), and atrial pacing at 100 bpm (e). In all the panels, the inflow velocity envelope is shown in *green* and the mitral valve closure time is represented by a *red-dashed vertical line*. Notice the truncation of the A wave for AVMIN, shortening the timing of atrial driven filling, and the fusion of the E and A waves for tachycardia



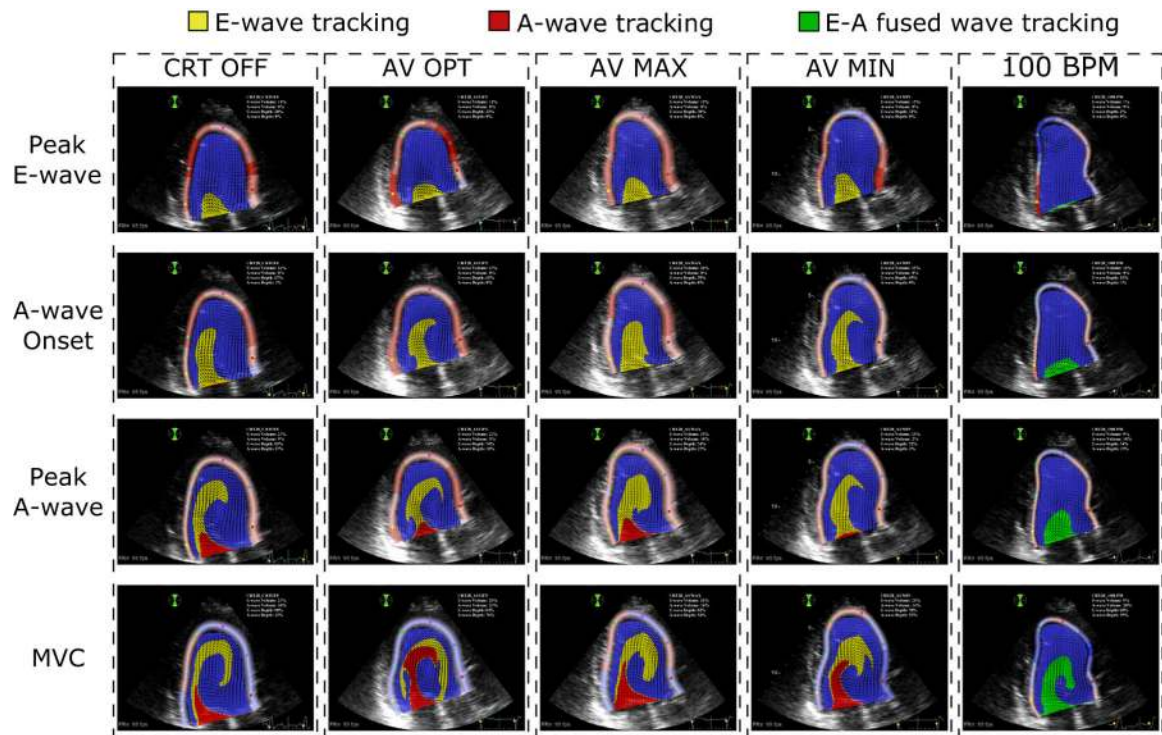


**Fig. 2.** Evolution of filling transport regions in the LV of the same patient shown in Figs. 1, 2. *Each column* represents a different CRT setting: **a** CRT-OFF, **b** AVOPT, **c** AVMAX, **d** AVMIN and **e** Tachycardia (100 bpm). *Each row* represents a different instant during diastole: the 1st, 2nd, 3rd and 4th rows correspond respectively to peak E-wave, A-wave onset, peak A-wave and mitral valve closing (MVC). In *each panel*, the *yellow* and *red* regions track respectively the fluid that enters the LV during the E-wave and the A-wave, whereas the *blue background* tracks the residual volume of blood that occupies the LV at the *onset* of diastole. Instantaneous velocity vectors are shown in *black*. In the Tachycardia setting the E/A-waves fusion is depicted in *green*. (Color figure online)

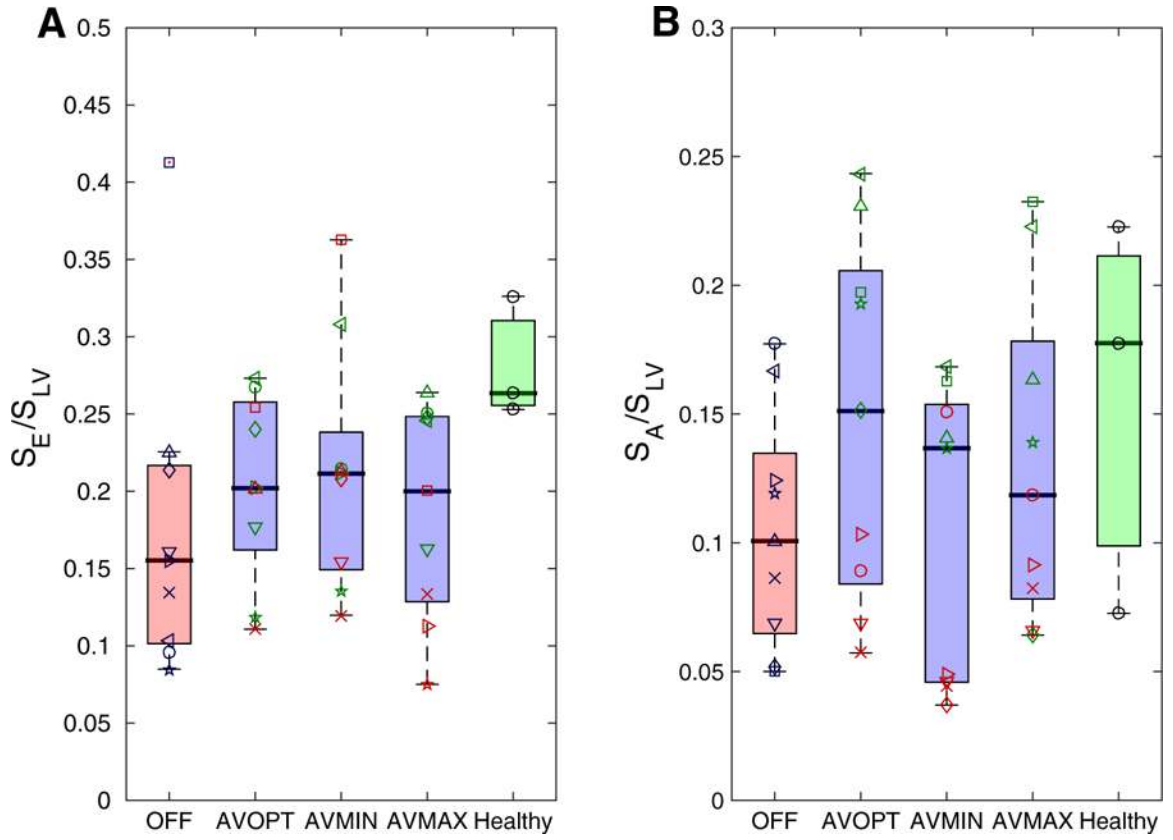


**Fig. 3.** %LV volume occupied by E-wave (a) and A-wave (b) filling transport at mitral valve closing in patients (N = 9) undergoing CRT with different AV delay settings, compared with healthy volunteers (N = 3). The data in *each column* are plotted as univariate scatter plots and summarized in the form of *boxplots*. In the patients, *red* and *blue boxplots* refer respectively CRTOFF and different AV delay cases. Each *symbol* type refers to a different patient, and is colored in *green* (*red*) if CRT makes the corresponding variable more (less) similar to the healthy subjects. The latter are represented by a *green boxplot*. (Color figure online)

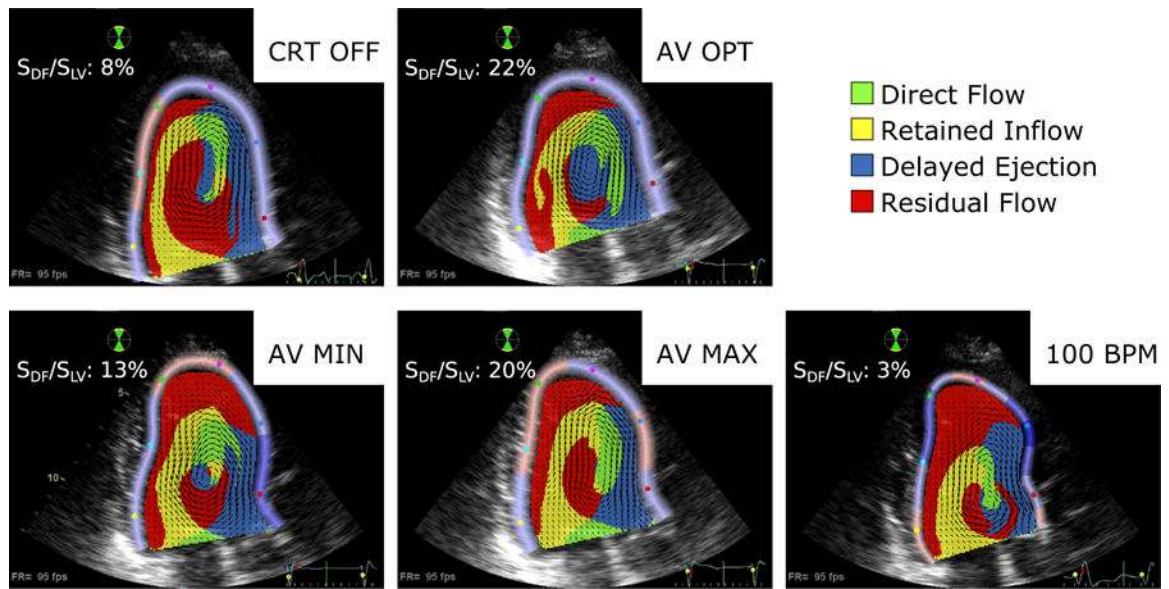


**Fig. 4.** End-diastolic distribution of different transport regions in the LV of the same patient shown in Figs. 1, 2, 3, plotted for different CRT settings (CRT OFF, AV OPT, AV MIN, AV MAX and Tachycardia). The different regions represented are direct flow (*green*), retained inflow (*yellow*), delayed ejection (*blue*) and residual flow (*red*). (Color figure online)

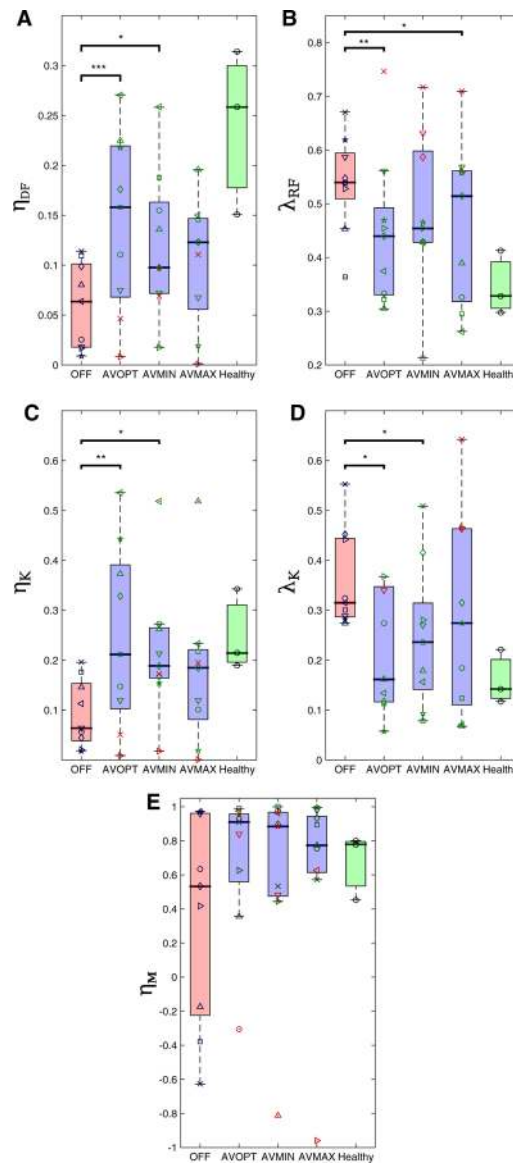


**Fig. 5.** Statistics of intraventricular blood redirection efficiency at aortic valve opening in patients (N = 9) undergoing CRT with different AV delay settings, compared with healthy volunteers (N = 3). **a** Fraction of LV volume that undergoes direct flow in the imaged plane,  $\eta_{DF} = S_{DF}/S_{LV}$ . **b** Fraction of LV occupied by residual volume in the imaged plane,  $\lambda_{RF} = S_{RF}/S_{LV}$ . **c** Fraction of total kinetic energy in the LV contained in the direct flow region,  $\eta_K = K_{DF}/K_{LV}$ . **d** Fraction of total kinetic energy in the LV contained in the residual volume,  $\lambda_K = K_{RF}/K_{LV}$ . **e** Net acceleration communicated to the direct flow region in the direction of the outflow tract, normalized by the total acceleration magnitude,  $\eta_M = (M_{DF} \cdot e_{LVOT})/|M_{DF}|$ . The data in *each column* are plotted as univariate scatter plots and summarized in the form of *boxplots*. In the patients, *red* and *blue boxplots* refer respectively CRTOFF and different AV delay cases. Each *symbol* type refers to a different patient, and is colored in *green (red)* if CRT makes the corresponding variable more (less)

similar to the healthy subjects. The latter are represented by a *green boxplot*. (Color figure online)

Author Manuscript

Author Manuscript

Author Manuscript

Author Manuscript

Table 1

Summary of study population data

ID	Age	Gender	H.R. (bpm)	EF (%)	CRT OFF	AVOPT (ms)	AVMAX (ms)	AVMIN (ms)	100 bpm
VOL1	73	F	60	71	NORMAL	-	-	-	-
VOL2	55	F	70	56	NORMAL	-	-	-	-
VOL3	66	M	59	71	NORMAL	-	-	-	-
CRT1 (○)	70	F	CRT dep.	52	Yes	110	200	70	No
CRT2 (□)	78	F	CRT dep.	38	Yes	110	180	70	No
CRT3 (◇)	59	M	CRT dep.	39	Yes	90	200	70	No
CRT4 (⊕)	62	M	CRT dep.	14	Yes	90	150	70	No
CRT5 (◁)	80	M	CRT dep.	51	Yes	110	170	70	Yes
CRT6 (▽)	62	F	CRT dep.	31	Yes	110	210	70	No
CRT7 (△)	57	F	CRT dep.	29	Yes	110	170	70	Yes
CRT8 (×)	65	F	CRT dep.	30	Yes	120	160	100	Yes
CRT9 (⊗)	59	M	CRT dep.	43	Yes	80	180	70	No

Three normal subjects (VOL1–3) and nine patients undergoing CRT (CRT1–9) were considered. Patient CRT7 is used as example in Figs. 1, 2, 3 and 5. Each patient is labeled with the symbol used to represent their data in Figs. 4 and 5

H.R. heart rate, EF ejection fraction, NORMAL normal volunteer, CRT dep CRT dependent



Intraclass correlation coefficient ( $R_{ic}$ ) and relative error (mean  $\pm$  std) of the reproducibility study

**Table 2**

Parameter	Intraobserver		Interobserver	
	$R_{ic}$	Relative error (%)	$R_{ic}$	Relative error (%)
$S_{DI}/S_{LV}$ ( $\eta_{DP}$ )	0.75	1 $\pm$ 20	0.85	17 $\pm$ 13
$S_{RI}/S_{LV}$	0.46	20 $\pm$ 26	0.51	14 $\pm$ 27
$S_{DE}/S_{LV}$	0.70	3 $\pm$ 34	0.69	22 $\pm$ 27
$S_{RF}/S_{LV}$ ( $A_{RF}$ )	0.68	14 $\pm$ 18	0.84	12 $\pm$ 23
$S_E/S_{LV}$	0.73	24 $\pm$ 22	0.77	24 $\pm$ 14
$S_A/S_{LV}$	0.53	11 $\pm$ 42	0.53	1 $\pm$ 39

SDF: Direct flow, SRI: Retained inflow, SDE: Delayed ejection, SRF: Residual flow and, SLV: Whole LV planar volumes.  $S_E/S_{LV}$  and  $S_A/S_{LV}$ : fraction of LV size occupied by the E and A waves

**Table 3**

Results of E and A wave tracking at mitral valve closing (average  $\pm$  standard deviation)

	OFF	AVOPT	AVMIN	AVMAX	100 bpm	NORMALS
$X_{E/L}$	0.81 $\pm$ 0.14	0.82 $\pm$ 0.12	0.83 $\pm$ 0.14	0.87 $\pm$ 0.11	0.51 $\pm$ 0.16	0.75 $\pm$ 0.08
$X_{A/L}$	0.45 $\pm$ 0.16	0.45 $\pm$ 0.23	0.30 $\pm$ 0.20	0.51 $\pm$ 0.22		0.47 $\pm$ 0.12
$S_{E/S_{LV}}$	0.18 $\pm$ 0.1	0.20 $\pm$ 0.06	0.21 $\pm$ 0.08	0.18 $\pm$ 0.07	0.15 $\pm$ 0.10	0.28 $\pm$ 0.04
$S_{A/S_{LV}}$	0.10 $\pm$ 0.05	0.15 $\pm$ 0.07	0.10 $\pm$ 0.06	0.13 $\pm$ 0.06		0.16 $\pm$ 0.08

$X_{E/L}$  and  $X_{A/L}$ : normalized apical position of each E and A waves.  $S_{E/S_{LV}}$  and  $S_{A/S_{LV}}$ : fraction of LV size occupied by the E and A waves

Average  $\pm$  standard deviation of relative end-diastolic flow fractions of the LV for the different CRT settings compared with reference values obtained by PCMRI [22, 23, 25]

**Table 4**

	OFF	AVopt	AVmin	AVmax	100 bpm	Healthy	Eriksson et al. [25]	Eriksson et al. [25]	Fredriksson et al. [24]	Bolger et al. [22]	Bolger et al. [22]
N	9	9	9	9	9	3	13	1*	10	17	1*
$S_{DI}/S_{LV}$ ( $\eta_{DP}$ )	$0.06 \pm 0.04$	$0.14 \pm 0.09$	$0.12 \pm 0.07$	$0.10 \pm 0.06$	$0.06 \pm 0.05$	$0.24 \pm 0.08$	$0.37 \pm 0.05$	0.08	$0.44 \pm 0.06$	$0.21 \pm 0.06$	0.04
$S_{RI}/S_{LV}$	$0.23 \pm 0.07$	$0.24 \pm 0.07$	$0.23 \pm 0.10$	$0.26 \pm 0.09$	$0.16 \pm 0.11$	$0.20 \pm 0.04$	$0.17 \pm 0.04$	0.25	$0.17 \pm 0.03$	$0.27 \pm 0.08$	0.31
$S_{DE}/S_{LV}$	$0.17 \pm 0.04$	$0.17 \pm 0.08$	$0.17 \pm 0.06$	$0.17 \pm 0.06$	$0.13 \pm 0.08$	$0.21 \pm 0.02$	$0.16 \pm 0.03$	0.28	$0.15 \pm 0.03$	$0.27 \pm 0.06$	0.26
$S_{RF}/S_{LV}$ ( $\lambda_{RF}$ )	$0.54 \pm 0.09$	$0.45 \pm 0.14$	$0.48 \pm 0.15$	$0.46 \pm 0.15$	$0.66 \pm 0.17$	$0.35 \pm 0.06$	$0.30 \pm 0.05$	0.37	$0.23 \pm 0.06$	$0.24 \pm 0.12$	0.39

SDF: Direct flow, SRI.: Retained inflow, SDE: Delayed ejection, SRF: Residual flow and,  $S_{LV}$ :Whole LV planar volumes \* in the results by Eriksson et al., Fredriksson et al. and Bolger et al. account for a patient with dilated cardiomyopathy

Flow kinematic efficiency parameters obtained at aortic valve opening (average  $\pm$  standard deviation)

**Table 5**

	OFF	AVopt	AVmin	AVmax	100 bpm	NORMALS
$\eta_K$	0.09 $\pm$ 0.07	0.25 $\pm$ 0.18	0.22 $\pm$ 0.13	0.18 $\pm$ 0.15	0.07 $\pm$ 0.09	0.25 $\pm$ 0.08
$\lambda_K$	0.36 $\pm$ 0.10	0.26 $\pm$ 0.21	0.25 $\pm$ 0.14	0.29 $\pm$ 0.20	0.49 $\pm$ 0.30	0.16 $\pm$ 0.05
$\eta_M$	0.37 $\pm$ 0.61	0.70 $\pm$ 0.43	0.60 $\pm$ 0.57	0.62 $\pm$ 0.61	0.76 $\pm$ 0.27	0.68 $\pm$ 0.20

$\eta_K$ : ratio of total kinetic energy in the volume of fluid that is focused into the direct flow region;  $\lambda_K$ : ratio of total kinetic energy in the volume of fluid that is focused into the residual flow region;  $\eta_M$  net acceleration transferred to the direct flow region in the direction of the LV outflow tract normalized with the total magnitude of this acceleration